Chapter 2

Raman studies at metal interfaces

Because of the very low Raman cross sections[1] (10^{-29} to 10^{-30} cm^2) of small, non-resonant[2] molecules, highly sensitive detection devices, strong laser power and a large quantity of target species, usually found in bulk solid or high-concentration liquid samples, or at high surface-area porous catalyst supports,[16, 17] are essential to carry out normal Raman spectroscopy (NRS). Other optical processes like Rayleigh scattering or fluorescence emission have much higher scattering probabilities. Surface scientists are nevertheless interested in carrying out Raman studies at smooth metal surfaces, where an adsorbate monolayer generally consists of around 10^{15} molecules, because this spectroscopic technique provides several advantages in comparison to other spectroscopies like infrared or fluorescence spectroscopy: It not only allows working in the visible regime, but also covers a broad spectral range from around -1000 cm^{-1} (anti-Stokes scattering) to 4000 cm^{-1} (Stokes scattering), only blocking out $\sim$ 200 cm^{-1} around the laser line (Rayleigh scattering). High-end Raman spectrometers reach resolutions better than 0.1 cm^{-1} and thus are capable of monitoring slightest band shifts due to adsorbate interactions or orientational changes at the interface. Fluorescence of the adsorbate is sufficiently quenched at a metal surface, so that Raman bands can clearly be detected without fluorescence interference, and their rich chemical information content is easily accessible.

[1] The scattering cross section is defined as the ratio between the power of the scattered radiation and the intensity of the incident beam, $\sigma = P_{sc}/I_{inc}$.

[2] Molecules with (non-)resonant vibrational transitions with respect to the excitation laser line are referred to as (non-)resonant molecules in this thesis.

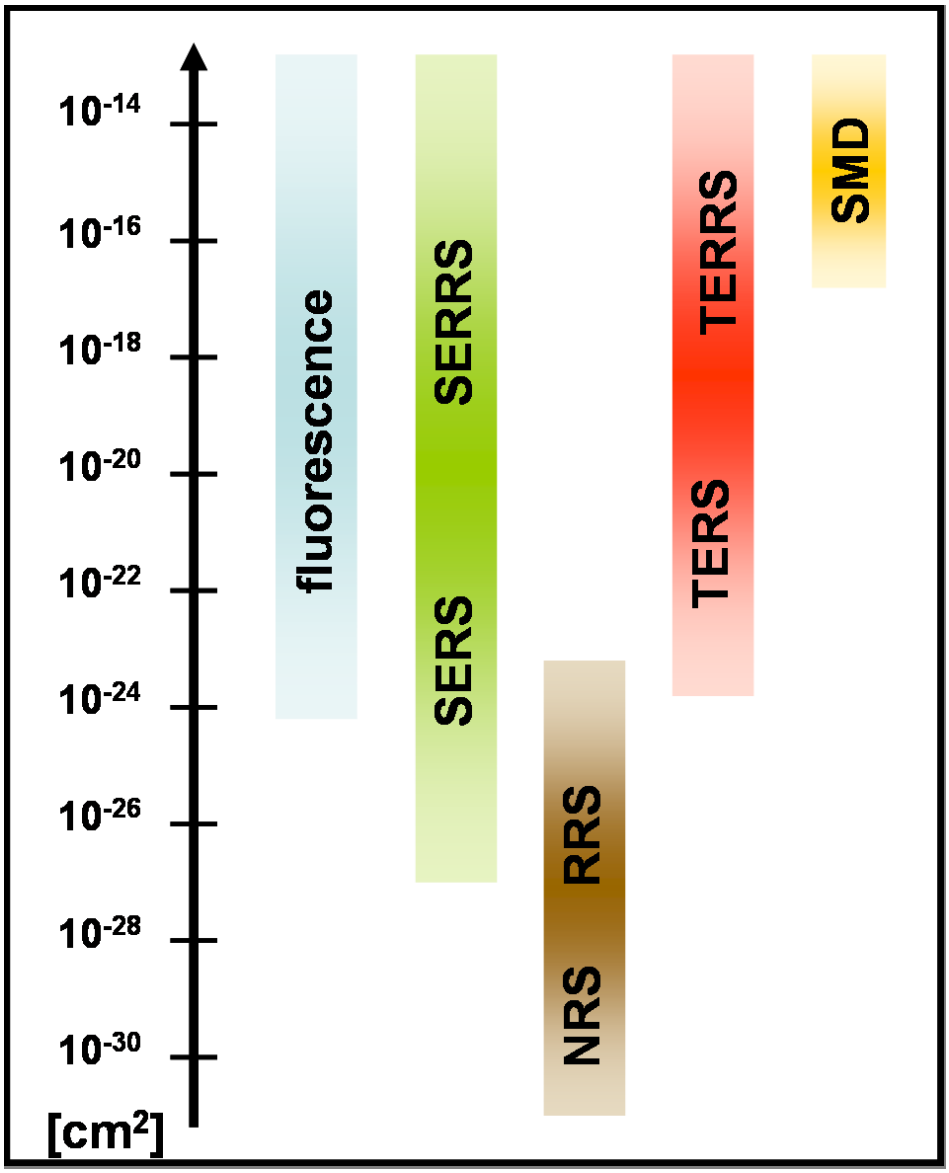

Figure 2.1: Overview of the differential cross-sections for a variety of spectroscopic techniques. NRS: Normal Raman spectroscopy; RRS: resonance Raman spectroscopy; SE(R)RS: surface-enhanced (resonance) Raman spectroscopy; TE(R)RS: tip-enhanced (resonance) Raman spectroscopy; SMD: single-molecule detection.

For an overview on spectroscopy cross sections, refer to Fig. 2.1. Resonance Raman spectroscopy increases the scattering cross section by several orders of magnitude. If, in addition, surface- or tip-enhancement is provided, the Raman cross section is further increased, reaching the fluorescence cross section and thus the single-molecule detection level.

2.1 Surface-enhanced Raman spectroscopy

Approximately 30 years ago, it was discovered that Raman studies at metal interfaces are indeed possible:[18–22] Employing a roughened Ag surface as a substrate would lead to very intense Raman scattering from the adsorbate due to the creation of a largely enhanced near-field. It was soon verified that the surface geometry of the substrate was responsible for the high band intensities, and not only the increased number of Raman scatterers present at an increased surface area in comparison to atomically smooth surfaces. Surface-enhanced Raman spectroscopy (SERS) makes use of the excitation of localized surface plasmons in rough metal surfaces. Any plasmon response induced in a planar surface cannot radiate because of the necessity of momentum conservation.[23] Thus, no surface-enhanced Raman spectra can be obtained from atomically smooth single-crystal surfaces, a major drawback of SERS. Mainly Ag, Au or Cu are employed, because the excitation of the LSPs of the coinage metals lies in the visible.[24] A schematic drawing that illustrates the SER configuration is found in Fig. 2.2. Laser light is focussed through an objective to a spot

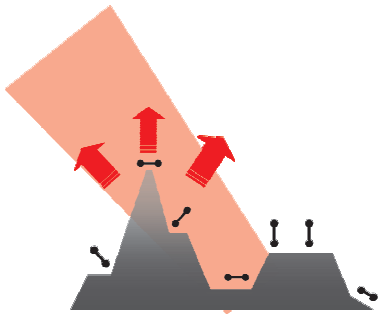

Figure 2.2: Excitation of localized surface plasmons in a rough coinage metal surface leads to a strongly enhanced electromagnetic field.

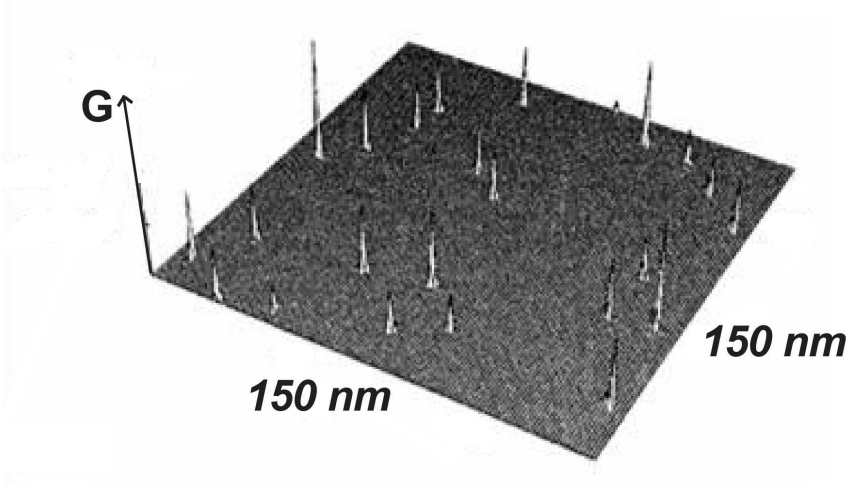

Figure 2.3: Theoretical modeling of an illuminated fractal silver surface shows that a strong near-field is found at discrete spots, the "hot spots". Figure reproduced from Ref. [25].

of approximately 2 μm diameter onto the rough sample surface. Adsorbed molecules experience the enhanced field which is created at surface corrugations. This gives rise to intense Raman scattering.

Calculations by Shalaev *et al.* (Fig. 2.3) showed that not the entire sample surface supports intense Stokes scattering of the adsorbate, but only very few spots of certain geometries: the "hot spots".[25] At these locations, an extremely enhanced field is created, which is responsible for the huge scattering intensities. It is an everlasting discussion which kind of substrate geometry actually produces the most intense field enhancement, and innumerable surface-enhanced Raman studies have been and are still being published on this subject. The interested reader is referred to recent reviews by, for example, Campion,[26] Shalaev,[27] Moskovits [28] or Kuncicky,[29] and references therein for detailed information.

One common point becomes apparent in all approaches: The gap between two nanoparticles seems to be the perfect location for a target molecule to experience the enhanced near-field and give rise to intense Raman scattering. Theoretical calculations usually make use of the "sphere model" (see, for example, Ref. [30]), in which the near-field created between two dipoles is considered (Fig. 2.4). The field is strongest at the

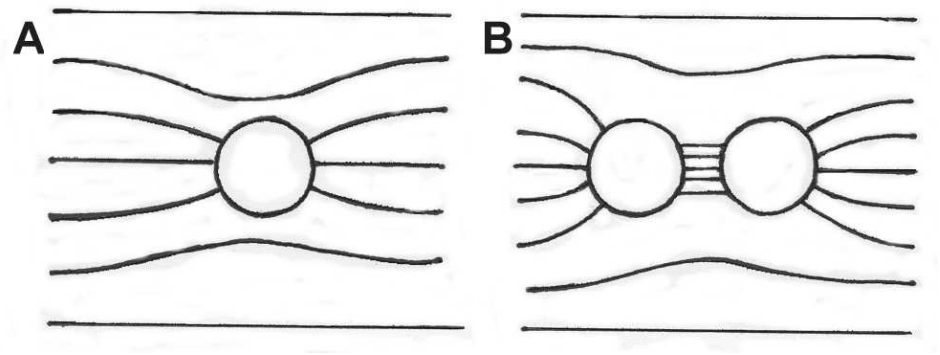

Figure 2.4: A: Electric field distribution near an isolated sphere. B: Electric field distribution near a two-sphere cluster. The near-field generated between two spheric dipoles is strongest at nearest dipole distance. The field lines arrive perpendicularly at the surface. Adapted from Ref. [30].

shortest distance between the two spheres, where all field lines arrive perpendicularly at the surface. The gap mode is red-shifted in comparison to the resonance mode of the isolated sphere.[31] A molecule sitting in the center between the two spheres couples strongly to this intensified gap mode and thus gives rise to enhanced Raman scattering. We will discuss the possible origin of the enhancement in Section 2.3 and give an introduction to localized surface plasmons in Section 2.4.

The Raman enhancement is calculated as the second power of field enhancement ($g = E/E_0$) of the incident photons, g_{in}^2, multiplied with the second power of the field enhancement of the scattered photons, g_{sc}^2, as a result of the metal particles acting as a nanoantenna for both the incident and scattered photons. If, in a first approximation, $g_{in} = g_{sc}$, we arrive at the famous g^4 Raman enhancement factor.

With SERS, extremely high Raman enhancement of 10^{14} to 10^{15} has been reported that is clearly sufficient for an analysis of a very low number of adsorbed molecules down to the single-molecule level.[32, 33] This especially hot topic – single-molecule Raman spectroscopy – will be addressed in Chapter 5 in detail.

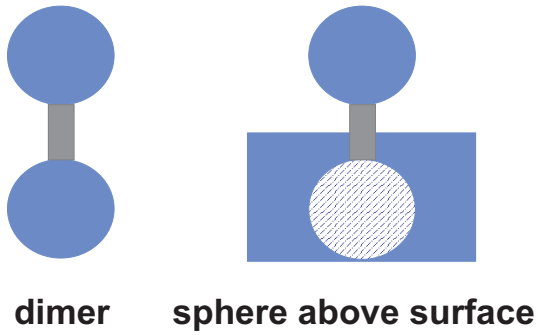

Figure 2.5: By bringing a metal tip close to a flat surface, an external roughness factor is created above, but extremely close to the smooth substrate. The resulting gap geometry is similar to the one between two spheres or two ridges on a rough surface.

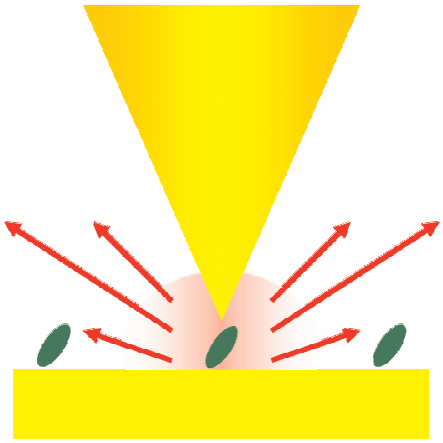

Figure 2.6: Excitation of localized surface plasmons in a metal tip leads to a strongly enhanced electromagnetic field in the cavity between tip and substrate surface.

2.2 Tip-enhanced Raman spectroscopy

There are two major drawbacks concerning SERS: The requirement of a rough sample surface and the restriction to the coinage metals (Ag, Cu, Au). Both can be overcome with tip-enhanced Raman spectroscopy, a slightly modified version of SERS, also known as apertureless scanning near-field optical microscopy. Rather than employing a deliberate two-particle geometry, an atomically smooth substrate is located underneath a scanning probe microscope (SPM) tip that acts as an "external roughness factor" (Fig. 2.5). The excitation laser light is focussed onto the very end of the sharp metal tip which is kept in close distance to the surface (approx. 1 nm). Localized surface plasmons or gap modes are excited in the apex of the tip and/or in the cavity between tip and sample, and only the molecules situated right underneath the tip in the enhanced field give rise to intense Raman scattering (Fig. 2.6). The tip serves as amplifying antenna for the incoming and outgoing electromagnetic waves, thus supporting extremely intense Raman scattering (Fig. 2.7A). If it is withdrawn, no Raman signal can be detected, as depicted in Fig. 2.7B.

Already in 1985, Wessel had the idea to "scan" a sample surface with a Ag nanoparticle that is controlled by piezo crystals.[12] He found it especially difficult to control the distance between particle and substrate, and suggested that a much easier control should be achieved by employing a metal STM tip in tunneling distance as a field enhancer - thus predicting the first TERS set-up realized 15 years later: The combination of a Raman spectrometer with an atomic force microscope, similar to the first fluorescence aSNOM set-up by Zenhausern *et al.*,[13, 14] was introduced by Zenobi and coworkers in 2000.[15] In a vertical alignment, the Ag AFM tip was placed over a dye layer dispersed on a glass support and illuminated from below. However, under these experimental conditions, only transparent samples can be employed. In order to be able to work with solid samples, like single crystal electrodes, the Pettinger group slightly modified the arrangement using an STM in a 60° configuration, which is described in detail in Chapter 3.[34]

With TERS, one of the main goals in surface science has been achieved: The combination of SPM and Raman spectroscopy allows the correlation of topographic and chemical information of the same surface region. The synergy of detailed insight in

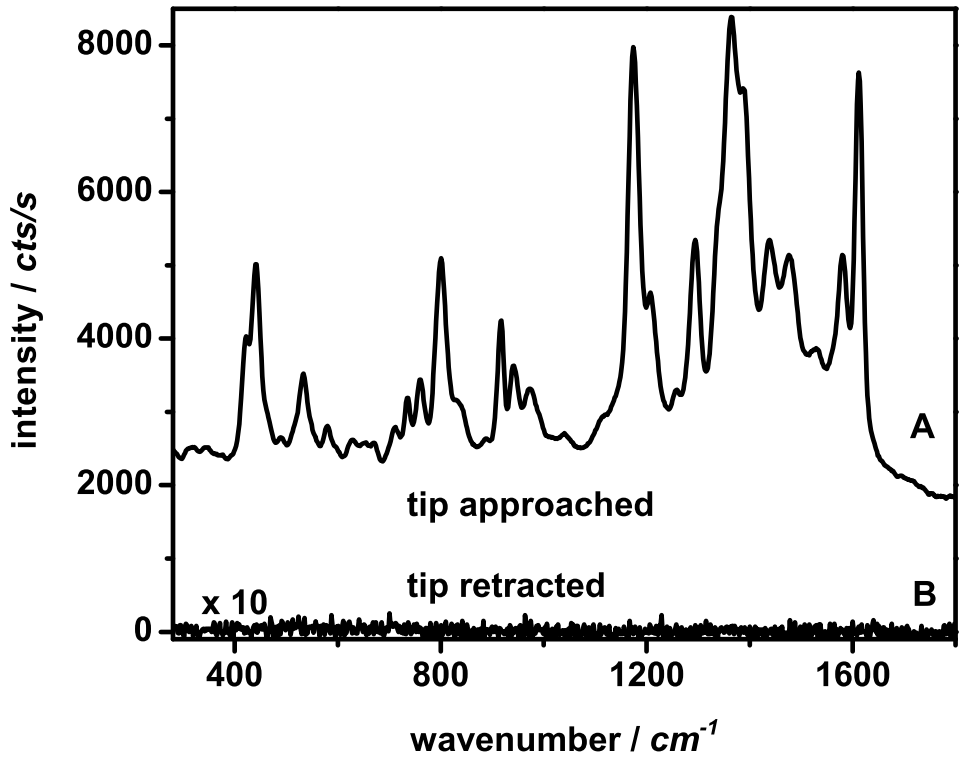

Figure 2.7: Raman spectra of MGITC obtained with different tip positions. A: Approaching the tip to $\sim d$= 1 nm, the typical Raman fingerprint is recorded. B: As long as the tip is fully retracted, no spectrum of a MGITC monolayer can be detected.

morphology and chemical nature of the target species greatly facilitates the characterization of interfaces at the nanometer scale and, in the combination, provides convincing evidence for the interpretation of the data. With the current set-up, Raman enhancements of 10^6 to 10^7 have been reached. Theory predicts a 10^8-fold Raman enhancement for a Au tip($r_{tip} = 20$ nm)/Au substrate system.[35] This means that large resonant target species with high(er) Raman cross sections can be detected down to the single-molecule level. A tip-enhanced resonance Raman (TERR) single-molecule study is presented in Chapter 5.

A wide variety of substrates and sample molecules have been employed in TERS up to date, with the experimental set-up still being limited to working in ambient conditions. However, modified set-ups for TERS in UHV and in electrochemical environment are currently being built and tested in the Pettinger group (described in Chapter 7).

2.3 Origin of field enhancement

Although numerous optical near-field studies have been published and Raman spectroscopy at interfaces is a commonly employed technique nowadays, the origin of the extreme Raman enhancement is still under discussion. Mainly, there are two types of enhancement that are ascribed more or less influence on the strong Raman scattering: the electromagnetic (EM) and the charge transfer (CT) mechanisms. In addition, a double-resonant (molecule and LSP in resonance) enhancement is also considered to play an important role.[36, 37]

The EM enhancement is associated with the resonant excitation of localized surface plasmons in the metal induced by the incident irradiation.[38, 39] Enhancement factors of 10^4 to 10^7 are attributed to this long-range effect, the created near-field stretching out several nanometers from the metal surface. The CT mechanism ("first layer effect"), which is said to contribute one or two orders of magnitude to the overall enhancement factor, is founded on the electronic interaction between metal and adsorbate.[40–42] Since such a charge-transfer process requires sufficient orbital overlap between the outermost layer of surface atoms and the adsorbate, it is a short-range effect that is most efficient for strongly bound (chemisorbed) molecules.

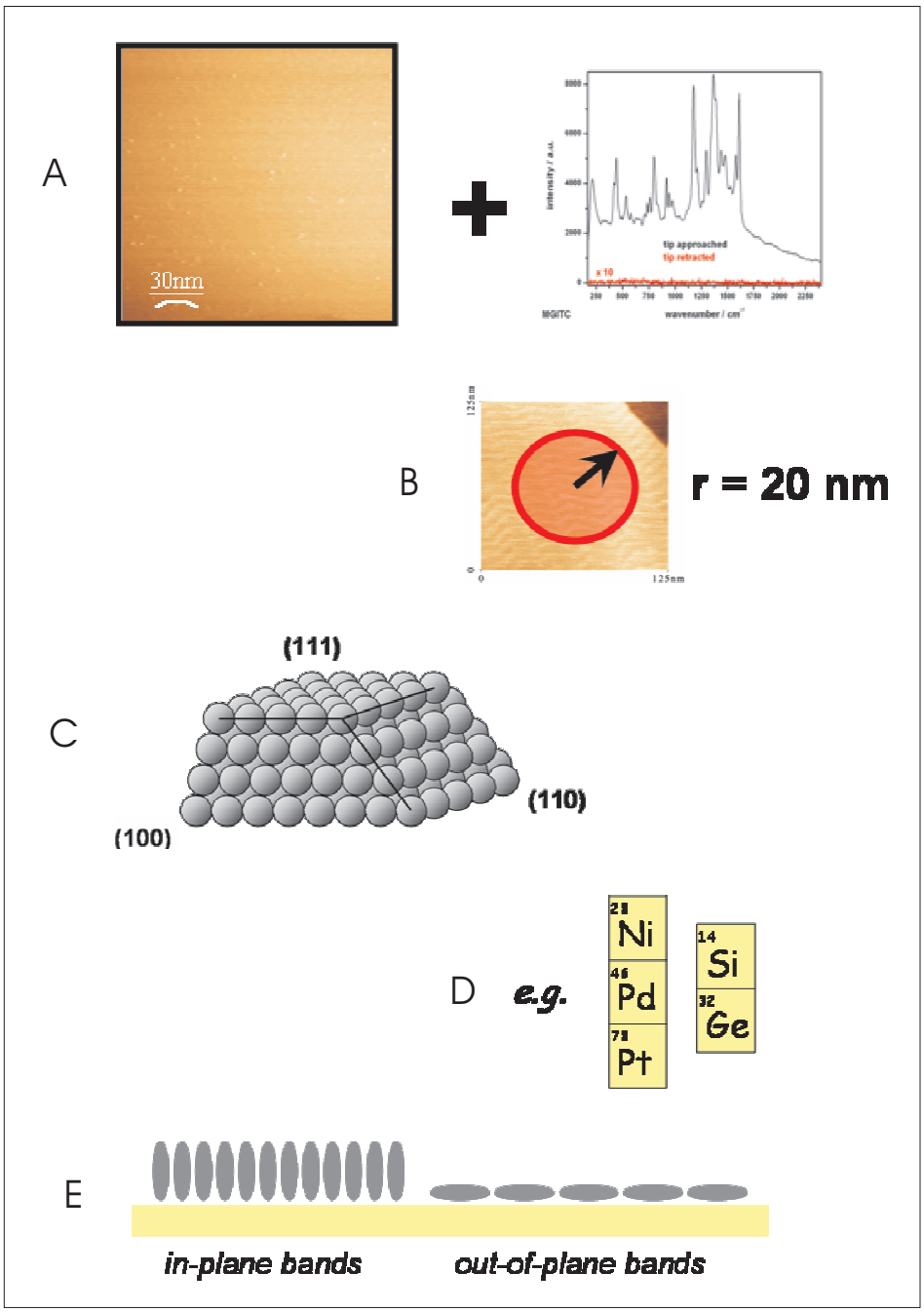

Figure 2.8: The main advantages of TERS are A) the combination of topographic and spectrographic information, B) nanometer optical resolution, C) use of atomically smooth single crystals, or D) any (semi)conductive substrate (insulators may of course be studied with AFM-TERS), and E) gain of structural and geometrical information on the sample.

For a detailed discussion on the different enhancement mechanisms, the interested reader is referred to articles by Schatz *et al.* (EM) and Otto *et al.* (CT) recently published in Topics of Applied Physics that describe the ongoing discussion in detail.[43]

Regarding this thesis, all experiments were performed with 632.8 nm laser light illuminating a Au STM tip, in resonance with the LSPs on the Au tip apex. The EM and resonant parts of the field enhancement are discussed in Chapter 5 for a resonant dye, MGITC, adsorbed at Au(111).

2.4 Localized surface plasmons

Since the electromagnetic enhancement is considered to be the dominant effect in the overall Raman enhancement, it is useful to have a deeper look at the underlying phenomenon, the excitation of localized surface plasmons.

Plasmons are the quasiparticles resulting from a quantization of plasma oscillations. These are collective longitudinal periodic oscillations of the free electron gas in a metal or semiconductor at optical frequencies. Surface plasmons are the plasmons confined to the interface of a material with a positive dielectric constant and a material with a negative dielectric constant, such as a metal.

Plasmons play a large role in the optical properties of metals. Electromagnetic waves with a frequency smaller than the surface plasmon frequency are efficiently reflected because the electrons screen the electric field. On the other hand, electromagnetic waves with a frequency above the surface plasmon frequency are transmitted, because the electrons cannot respond fast enough to screen them. For most metals, the surface plasmon frequency lies in the UV range. This explains the shiny metal surfaces caused by the reflection of light in the visible frequency regime. Surface plasmon frequencies in the infrared regime can be found for doped semiconductors. Of interest for tip-enhanced Raman spectroscopy are those metals, where the excitation of the surface plasmons lies in the visible frequency regime, such as the coinage metals. The surface plasmons of alkali metals are also excitable in the visible region, but such samples are difficult to handle in ambient conditions.

For the excitation of surface plasmons in a planar metal surface by p-polarized

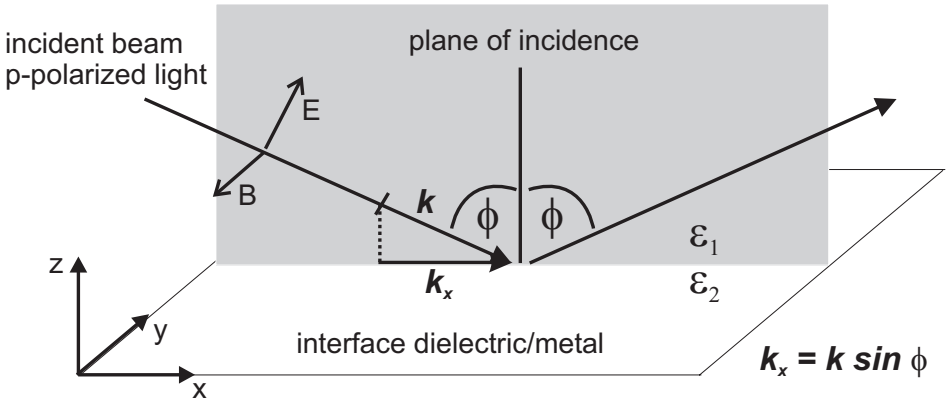

Figure 2.9: An incident beam at a planar metal surface at an angle ϕ to the surface normal and with a wavevector k possesses a momentum parallel to the surface, $k_x = k\,sin\phi$. If the light is travelling through air ($\epsilon_1 = 1$), it is reflected by the metal surface.

incident laser light, both energy and momentum conservation have to be fulfilled. Let us consider a laser beam with a wave vector k at an incident angle ϕ to the plane of incidence at a metal/dielectric interface with the dielectric constants ϵ_1 and ϵ_2 of the dielectric and the metal, respectively, like sketched in Fig. 2.9. The momentum parallel to the surface, k_x, is then defined as $k_x = k\,sin\phi$. With $\epsilon_1 = 1$, as it is the case for air, conservation of momentum and energy is not fulfilled, as shown in Fig. 2.10: The light curve (full red line) does not intercept the surface plasmon dispersion curve (black curve) at any point. Thus, the LSPs cannot be excited by the incident radiation.

In order to be able to excite the surface plasmons in a metal, momentum-matching techniques such as prism or grating coupling may be used. A configuration with a glass prism according to Otto or Kretschmann (Fig. 2.11),[44–46] makes use of the advantage of the sufficiently large dielectric constant ϵ_3 of the glass. In this way, the slope of the light curve (now $k_x = (\hbar\omega/c)\sqrt{\epsilon_3}$, dashed red line) is lowered so that it intersects the curve of the surface plasmons (Fig. 2.10). For a given wavelength and system parameters ϵ_1, ϵ_2 and ϵ_3, there is exactly one angle of incidence at which the LSPs at the metal/air interface are excited. Because of the energy transfer from incident photon to LSP, the reflectivity of the metal surface drops to nearly zero at this angle. This can be monitored in a simple experiment, where the reflectivity at a given wavelength of a thin metal film deposited on a prism with sufficiently high ϵ_3 is

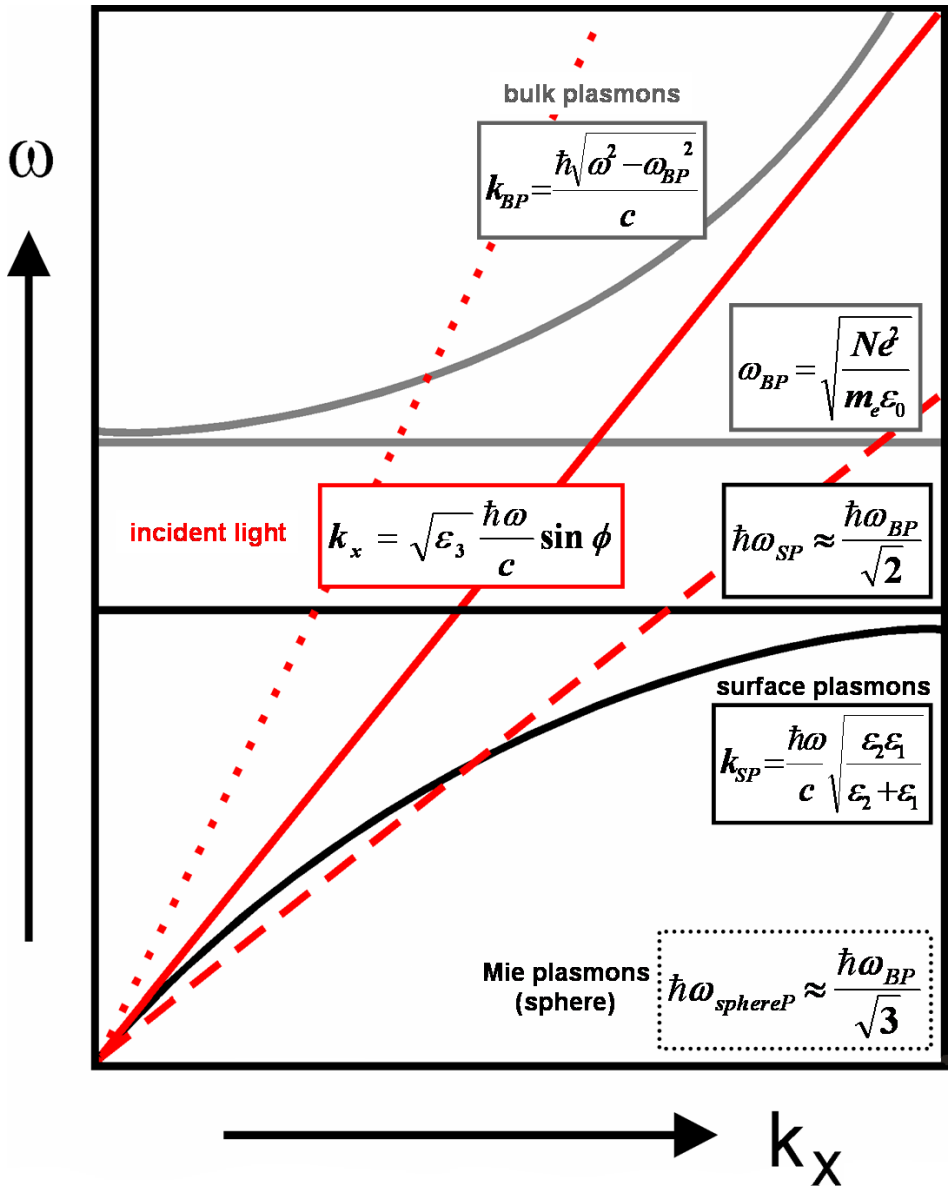

Figure 2.10: Dispersion curves for bulk and surface plasmons in a metal. An incident light beam travelling through air ($\epsilon_1 = 1$) does not intercept the plasmon curves and no excitation of (surface) plasmons can occur. Increasing the permittivity of the surrounding medium, i.e. employing a glass prism, lowers the slope of the light curve to allow intersection with the dispersion curve of the surface plasmons for a certain angle of incidence. Energy and momentum conservation are ascertained, and surface plasmons can be excited.

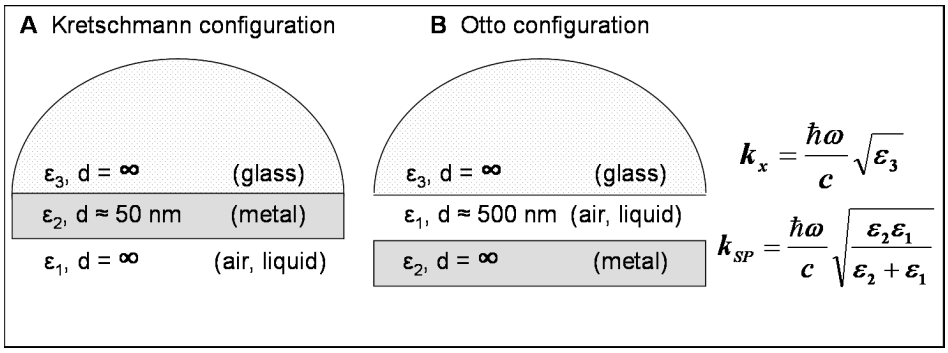

Figure 2.11: An experimental configuration with a glass prism enables the excitation of LSPs at a certain angle of incidence. In the Kretschmann configuration (Ref. [44]), the prism is covered with a thin metal film, whereas in the Otto configuration (Ref. [45]), a thin air or liquid layer is compressed between the glass and the metal. LSPs are excited at the metal air (or liquid) interface.

measured as a function of the incidence angle of the monochromatic excitation laser beam, as depicted in Fig. 2.12.[47] A clear dip in the reflectivity of the silver film is seen at 42.7°, where the excitation of the LSPs takes place. Alternatively, the angle could be kept constant and the reflectivity measured as a function of the incident wavelength.

Such experiments are employed to determine the film thickness or the refractive index of the interlayer (ϵ_1). One application are optical sensors for biomedical research, where smallest sample amounts are detected by a change in the reflectivity of the surface on which the sample is adsorbed (Kretschmann configuration, see Fig. 2.11A). Newest high-end multipass devices are able to lower the reflectivity of the film to 0.1%, enabling sensoring of target substances present at the metal surface in extremely low concentration.[48] The confinement of light to extreme small dimensions is often used in high-resolution lithography and microscopy.[49–51] A possible future application is also seen in optical data storage. Employing a near-field rather than a far-field read-out, the storage capacity of a conventional CD, for example, would largely increase.[52] Another example for the use of LSP resonances for ultrasensitive detection of adsorbates is described in this thesis: enhanced Raman spectroscopy.

In SERS, nonplanar interfaces with sufficiently large curvatures are used to support an efficient coupling of photons to surface plasmons. Periodicities in the surface profile can provide the missing momentum required to couple non-radiative plasmon

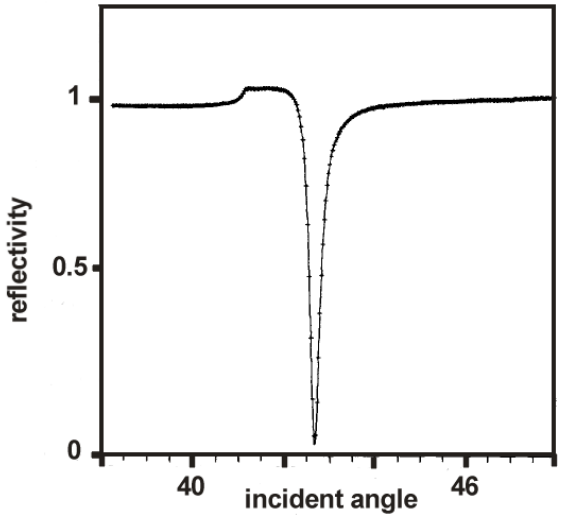

Figure 2.12: P-polarized eflectivity from a silver-coated prism of 632.8 nm He-Ne laser light showing the excitation of the LSPs as a deep reflectivity dip (adapted from Ref. [47]).

modes and photons. A significant increase in the coupling can be achieved with metallic structures of small curvature in the nanometer regime (clusters on a surface, or a metal tip) which introduce a "bandgap" in the propagation of plasmon modes, localizing them: The corrugation pitch provides just the required momentum to excite the plasmon mode. The decay channel of the surface plasmons, which are in this way localized, is switched off, the mode is trapped and can couple to the adsorbate. In the TERS case, the surface plasmons of the metal tip (sphere) and the surface plasmons of the (flat) substrate surface merge to a new LSP mode system (gap mode). If the incident laser light is in resonance with the LSP mode, it couples to it. The excited LSP mode has a strong near-field that is much enhanced in comparison to the incident field. The created enhanced field interacts with the adsorbate molecule, and, similarly, the scattered photon emerges from the molecule via the excitation of another LSP mode, again providing a strong enhancement for the scattering process. Incident and emitted photons both couple to the LSP modes in a similar strength and provide enhancement, thus resulting in the above-mentioned $g_{in}^2\, g_{sc}^2 \approx g^4$ enhancement factor (for $g_{in} \approx g_{sc}$) in enhanced Raman spectroscopy.

2.5 How far does the near-field reach?

2.5.1 Lateral resolution

Many different theories on the lateral extension of the near-field created at the tip-substrate cavity have been proposed, but, so far, none has been proven experimentally. In the following discussion, the extension of the near-field along the surface from the projection of the tip-center at the surface, x_0, is the enhanced-field radius, r_{ef}. The TERS radius, r_{TERS}, defines the area from which 1/e of the TER scattering intensity originates. The lateral Raman imaging resolution of the instrument is defined as $2\,r_{TERS}$.

The simplest approximation of the near-field distribution at the tip apex is a Heaviside step function, for which $r_{ef} = r_{tip}$. The lateral resolution is then defined by the curvature of the employed tip. More sophisticated theories agree that the near-field and resulting TERS radii indeed depend on the tip geometry, and also on the substrate employed and the tip-sample distance, but arrive at TERS radii much smaller than r_{tip}.

In the very first particle-enhanced publication, Wessel stated that the lateral resolution of the instrument reached $0.4\,r_{tip}$ for particle-sample distances smaller than 2 nm.[12] This approximation would give a 8 nm resolution for a tip with $r_{tip} = 20$ nm. Downes and Elfick recently published a calculation on a 20 nm Au tip at 1 nm distance to a Au surface and with this calculation arrived at the incredibly small value of 2.4 nm lateral resolution. This would mean that we could approach small particle dimensions in the optical resolution with TERS.[54]

Notingher *et al.* showed that the lateral extension of the TERS near-field varies significantly with the substrate material. For a Au tip with $r_{tip} = 20$ nm, the authors calculate a lateral resolution of 18.5 nm on a glass substrate and 8 nm on a Au substrate. The resolution is optimal for resonant metal-metal systems at close distances, where the field confinement is largest.[35]

A slightly more generous estimate of the lateral extension of the near-field can be obtained according to the well-known $1/R^3$ near-field distance dependence, as in detail described by Pettinger *et al.* in Ref. [53], leading to a $1/R^{10}$ distance dependence in

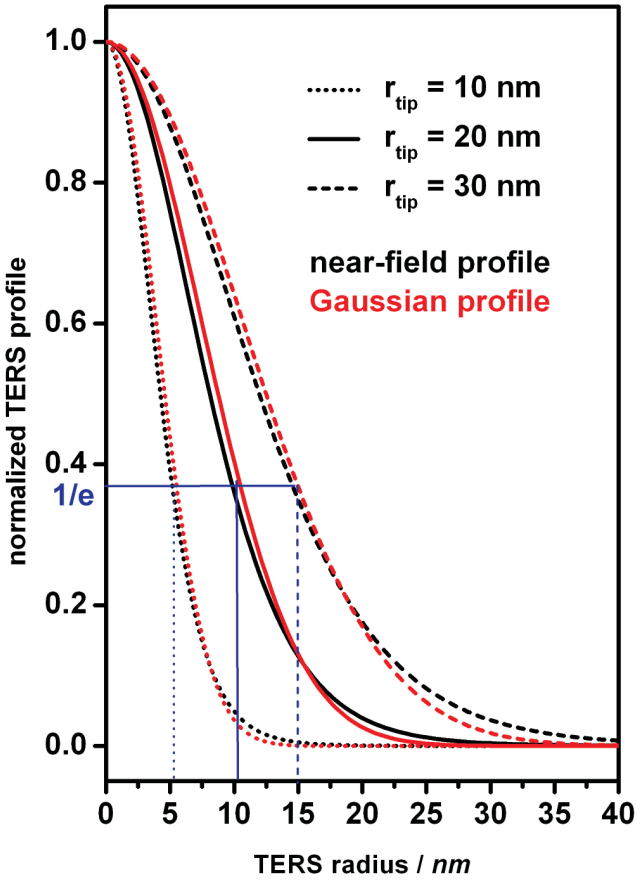

Figure 2.13: The lateral field distribution for a near-field profile ($[1-r^2/(r_{tip}+1)^2]^{-5}$) according to Ref. [53] shows a similar behaviour as a Gaussian profile. 1/e $r_{TERS} \approx 1/2r_{tip}$.

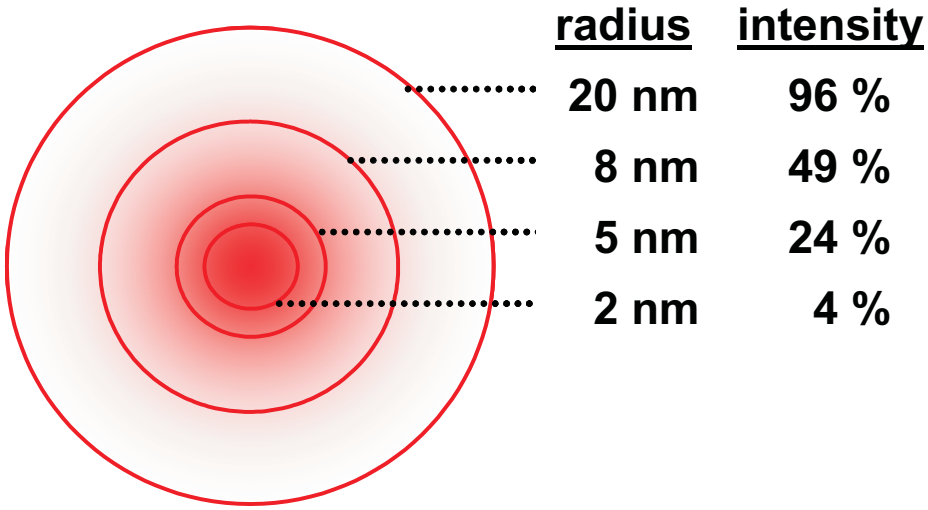

Figure 2.14: Schematic sketch of a Gaussian field distribution. The strongest field enhancement is found in the center, directly underneath the center of the tip apex. The lateral TER resolution (r_{TER}) is defined as the drop of the field intensity to 1/e. About 1/4 of the Raman signal originates from only 6% of the area!

the TERS case. As sketched in Fig. 2.13, the obtained curve nearly follows a Gaussian distribution. According to this near-field approximation, for a tip of 20 nm radius, one arrives at a lateral resolution of around 10 nm, or approximately half the tip radius.

Although the different theoretical approaches do not lead to identical values for the lateral resolution obtained by our standardly employed 20 nm curvature tip, they do agree in one point: The TER scattering radius is much smaller than the tip curvature, and, thus, $r_{TERS} = 1/2\, r_{tip}$ seems to be a safe approximation. Hartschuh *et al.* investigated carbon nanotubes with TERS.[55] Comparing topography images (AFM) to TERS images (r_{tip} = 10 nm), they determined the lateral resolution of their instrument to be 20 nm.

Experiments to examine the lateral field extension and distribution achieved upon our experimental conditions have not been carried out up to now. In addition to examination of an object of known size by Raman imaging, like carried out by Hartschuh *et al.*,[55] one could consider a lithography-type experiment in which the illuminated tip "writes" the characteristic shape of the near-field into a sensitive dye layer or pho-

toresist, either bleaching the dye molecules along its path or burning the photoresist. In order to "read" the field distribution, one could employ SPM to investigate the missing rows of molecules that have been destroyed during the writing process, or the width and depth profiles in the photoresist layer, which could give more precise information on the field intensity distribution. So far, however, our set-up does not permit precise tip positioning essential for such experiments, and also a conductive photoresist with a grain size < 1 nm has not been described in the literature.

The field distribution and lateral resolution of the instrument are of importance for the low adsorbate-coverage studies discussed in Chapter 5.

2.5.2 Vertical resolution

For the discussion of the tip-sample distance influence on the TER signal intensities (Chapter 4), we have to concentrate on the vertical extension of the enhanced field. Several groups have addressed this problem, and already in 1978, Rendell and Scalapino found that the field concentrated between a spherical dipole and a dielectric surface decreases with $\sqrt{2\,d\,r_{sphere}}$, where d is the distance between the sphere of radius r_{sphere} and the surface.[56] This model has been applied to SERS configurations, where most scattering intensity is obtained from molecules situated between two clusters or particles at close proximity. It can also be transferred to the case of TERS, where a sphere (the tip) is located shortly above a metal substrate.

Recent calculations by Festy *et al.*,[57] Brown *et al.* [58] and Notingher *et al.* [35]) consider an ellipsoidal tip shape and an extended 2D sample substrate. Depending upon the parameters employed (2D or 3D tip model, glass or metal substrate, excitation wavelength), the results vary considerably, as seen in Fig. 2.15.

Here, we consider a simple model (which results in a curve that fits our experimental data extremely well, as will be shown below), where the tip is approximated by a metal sphere above a metal surface (Fig. 2.16). Representing the tip by a sphere is a suitable model, since the resonance modes are highly localized in the tip-substrate cavity. A spherical model tip gives a rather good description of the most essential part of the tip in this situation, namely the curved apex facing the sample. The distance dependence of the scattering intensity is attributed to the distance dependence of the near-field

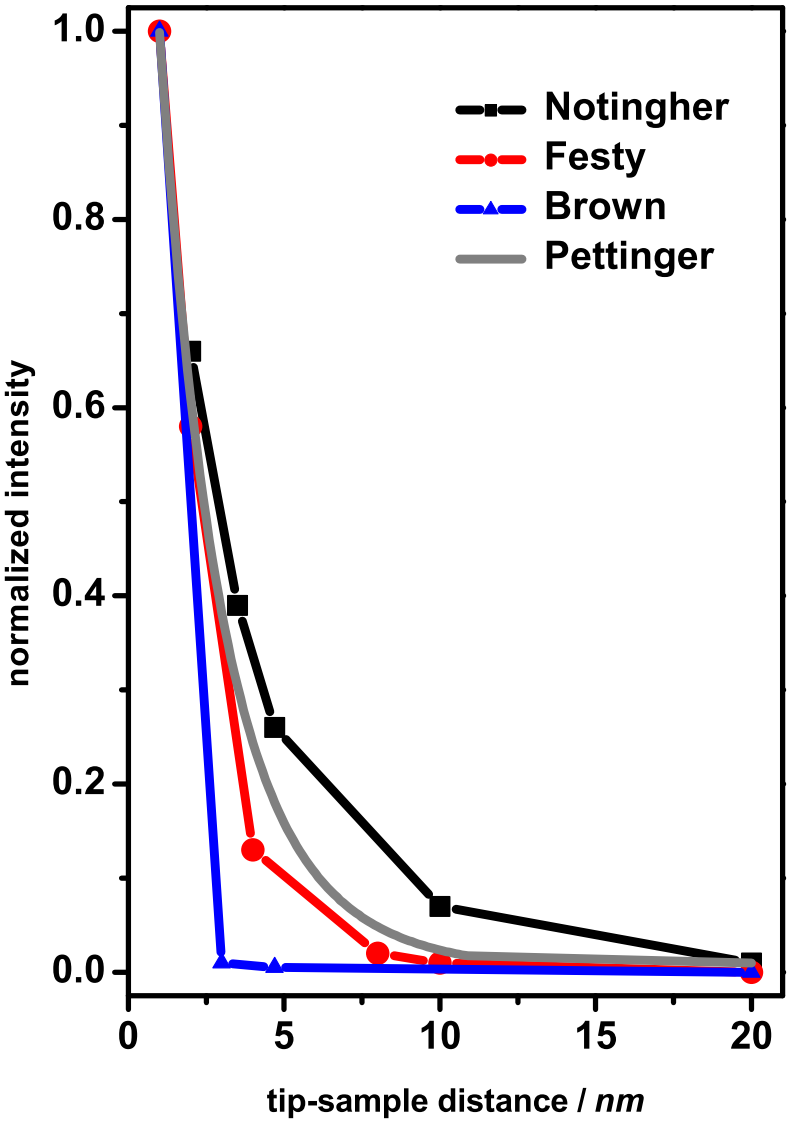

Figure 2.15: The different theories give very different curves for the vertical field extension or the tip-sample distance dependence. ■ Nothinger: Au tip with $r_{tip} = 20$ nm, glass substrate, 632 nm excitation wavelength, 3D; • Festy: Ag tip with $r_{tip} = 20$ nm, glass substrate, 631 nm excitation wavelength, 3D; ▲ Brown: Ag tip, Ag substrate, 514 nm excitation wavelength, 2D; — Pettinger model (3D) as described in Section 2.5.2.

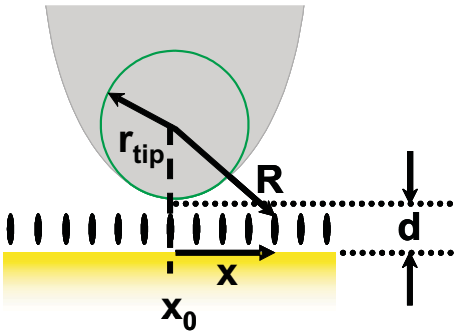

Figure 2.16: Simplified model of the tip-substrate cavity. The tip, which is located in tunneling distance $d = 1$ nm above the surface, is generally approximated by a sphere of the radius r_{tip}. The field at any point of distance x from underneath the tip center on the surface can be calculated for different tip radii (see text for details).

of an oscillating dipole induced in the tip (sphere). Thus, the EM-field enhancement g at the surface exhibits the distance dependence $g = g_0\, R^{-3}$, where R is the distance between the sphere center and the location of the molecule on the substrate and g_0 is the EM-field strength at unit distance.

In case of metal substrates, an additional image dipole must be considered (Fig. 2.17). To a first approximation, the superposition of the field components of dipole and image dipole results in a cancelling (doubling) of the field components parallel (perpendicular) to the surface. The overall enhancement of the Raman intensity is proportional to the combined enhancement of both processes, i.e. the enhancement of the intensities of incident and scattered light, $g_{in}^2\, g_{sc}^2$ (analogous to the enhancement in SERS [59, 60]), where g_{in}^2 describes the EM-field enhancement of the excitation processes and g_{sc}^2 accounts for the EM-field enhancement of the scattered radiation. Assuming similar enhancement levels for the incident and scattered light, $g_{sc}^2 \approx g_{sc}^2$ leads to the famous g_{ERS}^4 enhancement factor. As a consequence, the local Raman intensity enhancement I_{ERS} becomes proportional to g^4. After integration and normalization to the Raman intensity at $d = 1$ nm, the tip-sample distance dependence of TER scattering of a two-dimensional layer of molecules can be expressed in a simple analytical form:[53]

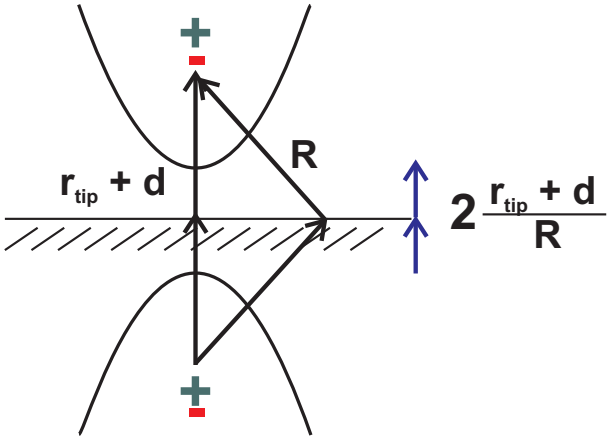

Figure 2.17: When employing a metal substrate, the dipole created in the metal tip apex will induce an image dipole in the surface. The field vector components parallel to the surface cancel out in a first approximation, but the ones perpendicular to the surface are doubled (see text for details).

$$I_{2D}^{ERS}(z \geq d) = (r_{tip} + d)^{10}(r_{tip} + z)^{-10}, \tag{2.1}$$

where z is the tip-sample distance (in tunneling contact $z = d$ =1 nm). The same relationship can be obtained if one takes into account the vectorial nature of the field components of two point dipoles; however, this derivation is beyond the scope of this Section. We will show in Chapter 4 that Eq. 2.1 excellently describes our experimental data on the Raman band intensity decrease with increasing tip-sample distance.